Shear flows and shear viscosity in a two-dimensional Yukawa system (dusty plasma)

V. Nosenko* and J. Goree

Department of Physics and Astronomy, The University of Iowa, Iowa City Iowa 52242

(May 21, 2004)

Abstract

The shear viscosity of a two-dimensional liquid-state dusty plasma was measured experimentally. A monolayer of highly charged polymer microspheres, with a Yukawa interaction, was suspended in a plasma sheath. Two counter-propagating Ar^+ laser beams pushed the particles, causing shear-induced melting of the monolayer and a shear flow in a planar Couette configuration. By fitting the particle velocity profiles in the shear flow to a Navier-Stokes model, the kinematic viscosity was calculated; it was of order 1 mm^2s^{-1}, depending on the monolayer's parameters and shear stress applied.

PACS number(s): 52.27.Lw, 82.70.Dd, 52.27.Gr

Typeset using REVTEX

*Electronic mail: vladimir-nosenko@uiowa.edu

A broad range of charged particle systems can be modeled as Yukawa systems that can have a liquid state; these include colloids, certain dense astrophysical plasmas, and strongly coupled dusty plasmas. A dusty plasma is a suspension of highly charged micron-size particles in a plasma. When these particles are confined, their mutual repulsion causes them to self-organize in a structure called a plasma crystal, which can be in a crystalline or liquid state.

Shear viscosity is a dynamic property of fluids required to describe shear flows and damping of waves. Recently, molecular dynamics (MD) simulations [1–3] and theory [4] have been used to predict the viscosity of a liquid Yukawa system. While viscosity is commonly measured in colloids, there are no reports of comparable measurements in dusty plasmas. A dusty plasma is much softer than a colloid, and between its particles it has only a rarefied medium consisting of free electrons and ions, as well as neutral gas, which applies a frictional drag to moving particles.

A plasma crystal is an analogue for molecular matter; the particles represent molecules [5], but they have the advantage of allowing direct imaging and thus a measurement of their individual positions and velocities [6]. Confinement of particles is provided by natural electric fields in the plasma. The particle suspension can be manipulated using various forces. In Ref. [7], ion drag forces were used to apply a shear stress that melted a two-dimensional (2D) crystallized dusty plasma. In Ref. [5], a 3D dusty plasma in a liquid state flowed past an obstacle where there was a shear. In those two experiments, experimenters had no direct control over the forces and the resulting shear. Here, we report an experiment using laser radiation to apply a controlled and localized shear stress to a monolayer lattice. The lattice melted, and we modeled the resulting velocity profile to measure the nonequilibrium viscosity. The geometry resembled a laminar planar Couette flow.

We used the apparatus of Ref. [8], with essentially the same parameters, including an Ar pressure of 5 mTorr. A monolayer of microspheres was suspended in the plasma. The particles had a diameter of 8.09 ± 0.18 μm [9] and a mass $m = 4.2 \times 10^{-13}$ kg. The particle suspension's diameter was $50 - 60$ mm. The interparticle potential in a monolayer like ours

was experimentally shown [10] to be nearly Yukawa: $U(r) = Q(4\pi\epsilon_0 r)^{-1}\exp(-r/\lambda_D)$, where Q is the particle charge and λ_D is the screening length. The particle suspension is characterized by $\kappa = a/\lambda_D$ and $\Gamma = Q^2/4\pi\epsilon_0 akT$, where T is the particle kinetic temperature. For liquids, the characteristic length a is the 2D Wigner-Seitz radius [11]; it is related to the lattice constant b for a perfect triangular lattice by $a = (\sqrt{3}/2\pi)^{1/2}b$. To vary a, κ, and Q, while keeping the plasma parameters constant, we used a different number of particles in each of three experiments, Table 1. We used the pulse technique of Ref. [12] to measure κ and Q.

Initially, our suspension was an undisturbed triangular lattice, Fig. 1(a). In this highly ordered state, the static structure factor $S(\mathbf{k})$ has the distinctive peaks of a hexagonal crystal, Fig. 1(b), and the pair correlation function $g(r)$ has many peaks and a correlation length of $r_{\rm corr} = (23 - 30)a$.

The particles were imaged through the top window by a video camera. We digitized movies of 256 frames at 30 frames per second. The 23.1×17.3 mm field of view included $370 - 770$ particles, Fig. 1(a). Coordinates x, y and velocities u_x, u_y were then calculated [6] for each particle in each frame.

To apply a shear stress in a planar Couette configuration, in an ordinary fluid one uses moving plates, but in our dusty plasma, Fig. 1(c), we used counter-propagating laser beams, as in Ref. [13], but with more laser power. Particles are pushed by the radiation pressure force F, which is proportional to an incident laser intensity [9]. An Ar^+ laser beam, with a power that was varied up to 3.41 W, was split in two. At their foci at the particle location, the laser beams had a diameter of 0.61 mm at the $1/e^2$ level. Two rapidly oscillating scanning mirrors rastered the beams into vertical sheets, which made footprints on the lattice by striking it at an angle of $6.7 - 8.8^\circ$ with respect to a horizontal plane. The sheets extended beyond the edges of the particle suspension.

In discussing our results, we first note that steady-state conditions in the velocity profiles developed within 3 s after turning on the laser. All the maps and profiles of particle velocity and temperature presented here were computed well after that time.

The particle velocity was always highest within the laser footprints. The velocity diminished elsewhere, with a profile that we will model.

Beginning with an undisturbed lattice, we applied increasing levels of shear stress, and we observed that the particle suspension passes through four stages: elastic deformation, defect generation while in a solid state, onset of plastic flow, and fully developed shear flow. We present data for the latter two stages. At the onset of plastic flow, Fig. 1(c), the particles hopped between equilibrium lattice sites. Domain walls developed, and they moved continuously. The crystalline order of the lattice in the shearing region deteriorated, broadening the peaks in the static structure factor $S(\mathbf{k})$ in Fig. 1(d). At still higher levels of shear stress, the lattice fully melted everywhere, and a shear flow developed, Fig. 1(e). The particle motion was highly irregular on a small scale compared to the interparticle spacing, but on a larger scale, it was like a laminar flow in a fluid. The liquid-like order of the particle suspension is clearly indicated by the diffusiveness of the structure factor $S(\mathbf{k})$ in Fig. 1(f). Particles were confined so that after flowing out of the field of view they circulated around the suspension's perimeter and re-entered the field of view, and the suspension did not buckle in the vertical direction. Within the field of view, the time-averaged flow was almost entirely in the x-direction.

We used a method of binning the velocity measurements u_x and u_y according to a particle's y position to compute spatial profiles $v_x(y)$ for the flow velocity, and $T_x(y)$ and $T_y(y)$ for the kinetic temperature. Within each bin, we computed moments of the velocity, and then time-averaged over 256 consecutive frames, beginning after a steady state was attained. This yielded $T_x(y)$ and $T_y(y)$ from the second moments of u_x and u_y, respectively, as shown in Figs. 1(c) and 1(e), and $v_x(y)$ from the first moment, as shown in Fig. 2(c). We used the region between the laser sheets to calculate a spatially and temporally averaged $< T_y >$, which we used to compute Γ_y. We use Γ_y and not Γ_x to characterize our system, because there was no external energy input in the y-direction. Separately, we also computed maps of velocity, $\bar{u}_x(x, y)$, which were time-averaged to reduce noise, Figs. 2(a) and 2(b).

At the onset of plastic flow, the velocity maps $\bar{u}_x(x, y)$ reveal interesting 120° zigzag

features, Fig. 2(a). This angle corresponds to a triangular lattice. The underlying movement of individual particles is best seen by viewing the movie [14].

In the fully melted condition, the velocity map in Fig. 2(b) has no significant variation in the x direction. In this shear flow, particles slip past their neighbors [14].

The flow velocity profile $v_x(y)$ in Fig. 2(c) was curved, unlike in a traditional planar Couette flow where $v_x(y)$ is linear with y. We attribute this curvature to the frictional drag exerted on particles by the gas. A balance between this drag in the x direction and the viscous transport of particle momentum mu_x in the y direction away from the laser footprints accounts for the observed steady-state velocity profile.

We modeled the velocity profile in the continuum approximation, using the Navier-Stokes equation with a term for the gas drag: $\partial\mathbf{v}/\partial t + (\mathbf{v}\nabla)\mathbf{v} = -\rho^{-1}\nabla p + (\eta/\rho)\nabla^2\mathbf{v} + [\zeta/\rho + \eta/(3\rho)]\nabla(\nabla\cdot\mathbf{v}) - \nu_d\mathbf{v}$. Here, the parameters for the continuum representing our particle suspension are $\mathbf{v}$, p, ρ, η, and ζ, which are the velocity, pressure, areal mass density, shear (dynamic) viscosity, and second viscosity, respectively, and ν_d is the gas friction. The ratio η/ρ is the kinematic viscosity, which has the same dimensions in 2D and 3D systems. Our flow has a symmetry $\partial/\partial x = 0$ and $v_y = 0$. The Navier-Stokes equation is then reduced to $\partial^2 v_x(y)/\partial y^2 - (\nu_d\,\rho/\eta)v_x(y) = 0$ and $p = const.$

We will compare our results to a theoretical velocity profile $v_x^{th}(y) = [(V_1 + V_2\,\mathrm{e}^{2\alpha h})\mathrm{e}^{\alpha y} - (V_2 + V_1\,\mathrm{e}^{2\alpha h})\mathrm{e}^{-\alpha y}]/(\mathrm{e}^{3\alpha h} - \mathrm{e}^{-\alpha h})$, where $\alpha = \sqrt{\nu_d\,\rho/\eta}$ and $2h$ is the distance between the laser sheets. We used the boundary conditions $v_x(-h) = -V_1$ and $v_x(h) = V_2$; if $V_1 = V_2 = V$, the theoretical profile simplifies to $V\sinh(\alpha y)/\sinh(\alpha h)$. Here we have ignored the spatial dependence of η/ρ, thereby neglecting the temperature gradient in the shear flow. As $\nu_d \to 0$, the solution approaches a linear velocity profile, as for a planar Couette flow. The gas drag $\nu_d \neq 0$ gives the steady-state velocity profiles a curvature depending on viscosity; this allows us to calculate the viscosity from the profiles, if ν_d is known.

We fit our experimental velocity profiles in Fig. 2(c) to theory using experimental values of V_1 and V_2 and a single free parameter α. We then calculated the kinematic viscosity $\eta/\rho = \nu_d\,\alpha^{-2}$ using the known value of Epstein gas drag $\nu_d = 0.87\ \mathrm{s}^{-1}$ for our experimental

conditions [9]. The resulting curves fit our profiles well.

Our main experimental result is the kinematic viscosity η/ρ of our particle suspension, Fig. 3(a). Its value is of order 1 $\mathrm{mm^2 s^{-1}}$, which is comparable to η/ρ for both a 3D Yukawa system and liquid water [1–5]. For a given value of κ, the parameter we varied was the applied laser power; increasing this power caused the shear stress to increase and Γ_y to decrease, so that these two parameters were not varied independently.

A prominent feature of Figs. 3(a) and 3(b) is a broad minimum in the viscosity. The minimum occurs in the range $70 < \Gamma_y < 700$. In 3D Yukawa systems, there is also a minimum, and the value of Γ for this minimum depends on κ [1–4].

We next consider some of the assumptions in our model and validate them using our experimental results. The weak dependence of viscosity on Γ_y in the range $70 < \Gamma_y < 700$ validates our neglecting the temperature gradient, but only in this range of Γ_y; our data points outside this range are less reliable, due to this assumption. The Reynolds number of our shear flow was $R = V_1 h/(\eta/\rho) = 0.7 - 17$; values this low typically indicate a laminar flow, validating that assumption in our model.

We have also assumed that the neutral gas does not flow and entrain the particles. This is true because the gas-gas collision mean free path of 15 mm was of the order of the entire suspension's size, and the particles filled only a tiny solid angle. Thus, a gas atom that was struck by one moving particle was unlikely to strike another.

The good fit in Fig. 2(c) suggests that the Navier-Stokes model, which is a continuum model that does not describe motion of individual molecules, works well even when the ratio of the shearing region width $2h$ to the Wigner-Seitz radius a is as small as 17 to 24, as it was in our experiment. In Ref. [1], tests suggested that validity of the Navier-Stokes model requires that the length scale $2h$ of the system exceed both the interparticle mean free path λ_{mfp} and r_{corr}. Both of these conditions are satisfied for our experiment. We validate the $2h > \lambda_{\mathrm{mfp}}$ condition by observing that $2h/a$ was in the range $17 - 24$ in our experiment, and judging that $\lambda_{\mathrm{mfp}} \approx a$, based on the movies of the particle motion [14]. We validate the $2h > r_{\mathrm{corr}}$ condition using the pair correlation results, yielding $2h/r_{\mathrm{corr}} = 3.0 - 9.4$ for all

data points except for two with $2h/r_{\rm corr} = 2.5 - 2.9$; for these, $\Gamma_y \geq 1000$. The latter two data points, which are for a mostly solid suspension, are therefore less reliable.

However, the Navier-Stokes equation cannot be used inside the laser footprints, where the shear stress is applied, because this region is very narrow, less than an interparticle spacing. For this reason, we did not extend our fits into the footprints. In general, if the Navier-Stokes equation fails to apply, one cannot expect the usual relation, that the shear stress is the product of the dynamic viscosity and shear rate, to apply.

Our experiment suggests a need for a theory or simulation for the viscosity of a 2D Yukawa system. The only previous work, to our knowledge, is for a 3D Yukawa system [1–4].

We thank B. Liu, J. Marshall, R. Merlino, and F. Skiff for valuable discussions. This work was supported by NASA and DOE.

REFERENCES

[1] K.Y. Sanbonmatsu and M.S. Murillo, Phys. Rev. Lett. **86**, 1215 (2001).

[2] G. Salin and J.-M. Caillol, Phys. Rev. Lett. **88**, 065002 (2002); Phys. Plasmas **10**, 1220 (2003).

[3] T. Saigo and S. Hamaguchi, Phys. Plasmas **9**, 1210 (2002).

[4] G. Faussurier and M.S. Murillo, Phys. Rev. E **67**, 046404 (2003).

[5] G.E. Morfill *et al.*, Phys. Rev. Lett. **92**, 175004 (2004).

[6] A. Melzer *et al.*, Phys. Rev. E **62**, 4162 (2000).

[7] U. Konopka *et al.*, Phys. Rev. E **61**, 1890 (2000).

[8] V. Nosenko *et al.*, Phys. Rev. Lett. **92**, 085001 (2004).

[9] B. Liu *et al.*, Phys. Plasmas **10**, 9 (2003).

[10] U. Konopka, G.E. Morfill, and L. Ratke, Phys. Rev. Lett. **84**, 891 (2000).

[11] G.J. Kalman *et al.*, Phys. Rev. Lett. **92**, 065001 (2004).

[12] V. Nosenko *et al.*, Phys. Rev. Lett. **88**, 135001 (2002).

[13] W.-Y. Woon and L. I, Phys. Rev. Lett. **92**, 065003 (2004).

[14] http://dusty.physics.uiowa.edu/∼goree/mov/sh.html

FIGURES

FIG. 1. Particle suspension at three levels of shear stress applied by a pair of counter-propagating laser sheets in a planar Couette configuration. Panels (a), (c), and (e) are top views with shear stress that is zero, moderate, and high, respectively. The snapshot of the undisturbed suspension (a) shows a highly ordered triangular lattice. At the onset of plastic flow (c), particle trajectories reveal localized hopping. In a fully developed shear flow (e), the trajectories show particles moving significantly everywhere. Profiles of the inverse particle temperature T_x^{-1} and T_y^{-1} are shown in the insets. The static structure factor $S(\mathbf{k})$ was computed as the Fourier transform, with a Hanning window, of the raw bitmap images as in (a). The peaks in $S(\mathbf{k})$ are distinctive for an undisturbed lattice (b); they are broadened and then diffuse at progressively higher levels of shear (d),(f). The particle suspension's parameters here and in Fig. 2 correspond to Experiment 1 in Table 1. We calculated η, $< T_y >$, and Γ_y using data in the range $-h < y < h$.

FIG. 2. Particle velocity data. Map (a), averaged over 64 frames at the onset of plastic flow, shows particle movement localized near the laser footprints. Map (b), averaged over 256 frames at the highest laser power, shows a fully developed shear flow that has no variation with x. Experimental profiles (data points) (c) are with fits to the Navier-Stokes model (curves), as used to calculate the kinematic viscosity of the particle suspension.

FIG. 3. Results for kinematic viscosity η/ρ, as functions of the shear stress (a) and coupling parameter Γ_y (b). The latter two parameters were not varied independently, but were related as shown in (c). There is a broad minimum in viscosity in the range $70 < \Gamma_y < 700$. In (b), to allow comparison to theory, we normalized the viscosity as $\eta^* = \eta/(\rho\omega_{pd}\, a^2)$, where $\omega_{pd} \equiv [Q^2/2\pi\epsilon_0 m a^3]^{1/2}$ for two dimensions [11].

TABLES

TABLE I. Parameters of the particle suspension measured without any shear flow, for three experiments.

	1	2	3
Wigner-Seitz radius a (mm)	0.402	0.449	0.580
κ	0.36	0.42	0.53
Q/e	-11 940	-13 840	-16 360
$\omega_{pd} \equiv [Q^2/2\pi\epsilon_0 m a^3]^{1/2}$ (s^{-1})	49.2	48.2	38.8

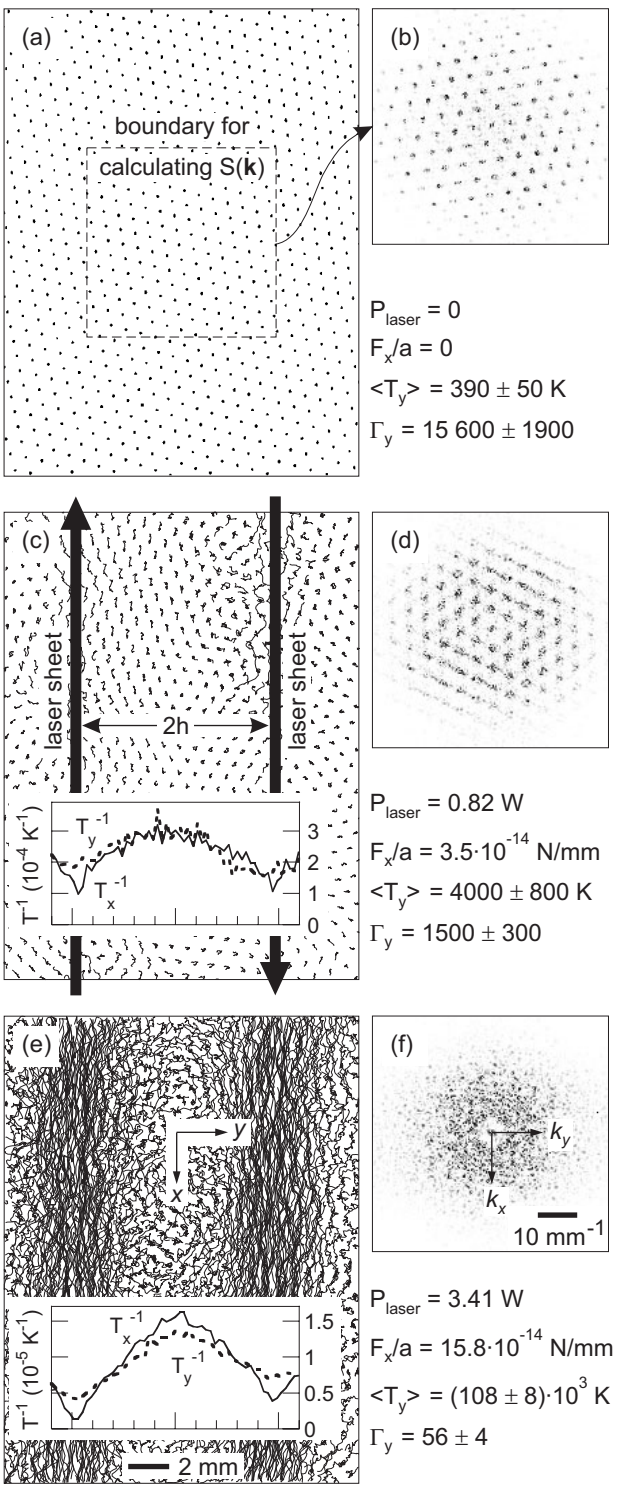
(a)
boundary for
calculating S(k)
(b)
P_laser = 0
F_x/a = 0
<T_y> = 390 ± 50 K
Γ_y = 15 600 ± 1900
(c)
laser sheet
2h
laser sheet
T_y^-1
T_x^-1
T^-1 (10^-4 K^-1)
3
2
1
0
(d)
P_laser = 0.82 W
F_x/a = 3.5·10^-14 N/mm
<T_y> = 4000 ± 800 K
Γ_y = 1500 ± 300
(e)
y
x
T_x^-1
T_y^-1
T^-1 (10^-5 K^-1)
1.5
1
0.5
0
2 mm
(f)
k_y
k_x
10 mm^-1
P_laser = 3.41 W
F_x/a = 15.8·10^-14 N/mm
<T_y> = (108 ± 8)·10^3 K
Γ_y = 56 ± 4

Fig. 1

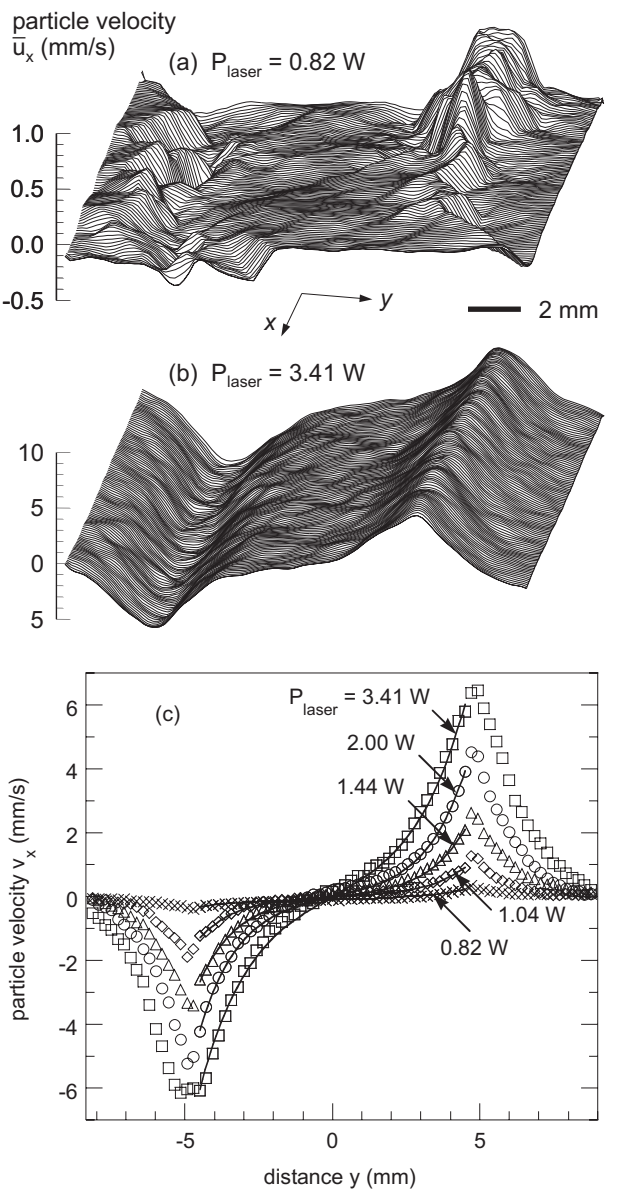
particle velocity
$\bar{u}_x$ (mm/s)
(a) P_{laser} = 0.82 W
1.0
0.5
0.0
-0.5
y
x
2 mm
(b) P_{laser} = 3.41 W
10
5
0
5
(c)
P_{laser} = 3.41 W
2.00 W
1.44 W
1.04 W
0.82 W
particle velocity v_x (mm/s)
6
4
2
0
-2
-4
-6
-5
0
5
distance y (mm)

Fig. 2

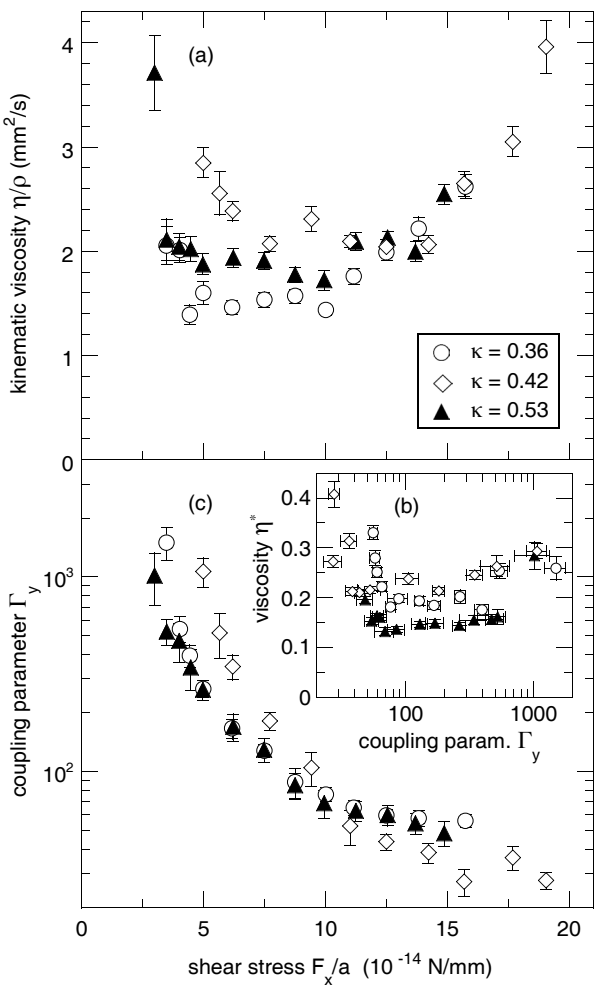
(a)
kinematic viscosity η/ρ (mm²/s)
κ = 0.36
κ = 0.42
κ = 0.53
(c)
(b)
coupling parameter Γy
viscosity η*
coupling param. Γy
shear stress Fx/a (10 -14 N/mm)

Fig. 3